SLAC-PUB-16971

Warm dense matter demonstrating non-Drude conductivity from observations of non-linear plasmon damping

B. B. L. Witte,[1,2] L. B. Fletcher,[1] E. Galtier,[1] E. Gamboa,[1]
H. J. Lee,[1] U. Zastrau,[3] R. Redmer,[2] S. H. Glenzer,[1] and P. Sperling[1,3]

[1]*SLAC National Accelerator Laboratory, 2575 Sand Hill Road, MS 72 Menlo Park, CA 94025 USA*
[2]*Institut für Physik, Universität Rostock, 18051 Rostock, Germany*
[3]*European XFEL, Holzkoppel 4, 22869 Schenefeld, Germany*

(Dated: April 30, 2017)

We present simulations using finite-temperature density-functional-theory molecular-dynamics to calculate the dynamic electrical conductivity in warm dense aluminum. The comparison between exchange-correlation functionals in the PBE and HSE approximation indicates evident differences in the density of states and the dc conductivity. The HSE calculations show excellent agreement with experimental LCLS x-ray plasmon scattering spectra revealing plasmon damping below the widely used Random Phase Approximation. These findings demonstrate non-Drude-like behavior of the dynamic conductivity that needs to be taken into account to determine the optical properties of warm dense matter.

PACS numbers: 52.25.Os, 52.35.Fp, 52.50.Jm, 78.70.Ck

The understanding of dissipative effects in systems of charged particles is one of the key problems in plasma physics [1, 2]. For dilute systems the linearized Boltzmann equation describes the transport properties adequately and damping of collective plasma modes can be understood by collisionless dissipative processes known as Landau damping. However, for dense plasmas a more complex behavior beyond the established plasma models, e.g., Drude and Landau, is anticipated due to strong correlations and quantum effects inherent under those conditions.

The treatment of non-linear effects is a particular fundamental challenge of mathematical and experimental plasma physics [3–6]. For instance, the damping of the collective electron density fluctuations (plasmons) will be modulated by additional collisional dissipations in warm dense matter (WDM). However, collisions and electronic excitations have to be treated in such a regime within a suited non-perturbative approach based on, e.g., density functional theory (DFT). Therefore, a close connection between dissipative effects and the damping behavior of plasmons is expected in WDM which will become manifest in the measurement and interpretation of thermal and electrical conductivities in terms of, e.g., the Lorenz number. The results are highly relevant for understanding the magnetic field generation in the interior of planets [7–10] and the study of fusion plasmas [11–13].

The challenge for the WDM regime is apparent from long-standing discrepancies between theoretical models and measurements of the electrical conductivity [14–25]. The theoretical studies are complex and include screened Coulomb forces that dominate interactions between ions while electrons are partially to fully degenerate. In particular, the electron-electron interactions result in non-local Pauli repulsions that can be included in analytical models [26, 27] and simulations [25, 28–30] externally. However, their predictability suffers from the lack of accurate physical models of these multi-body interaction processes. It is thus important to test recent theoretical studies [31–38] with accurate measurements of, e.g., the dynamic structure factor (DSF). The DSF is a central quantity to calculate transport properties [39].

The Linac Coherent Light Source (LCLS) [40–42] provides 10^{12} x-ray photons in a narrow bandwidth, $\Delta E/E = 10^{-4}$, per pulse allowing high signal-to-noise measurements [26] of the DSF [22]. These precision x-ray scattering studies determine the response of matter produced by the x-ray beam itself or by laser drivers [42]. In the forward scattering regime, the scattering spectra provide the collective plasmon (Langmuir) oscillations [39, 43]. These observations determine dissipative effects including Landau damping and binary collisions. First experimental studies [22] have demonstrated that existing theoretical models using perturbative approximations [43–46] are not suitable to describe the scattering data [22]. These findings demonstrate the need to develop theoretical models that go beyond the Random Phase Approximation (RPA) to accurately include electronic excitations and non-linear plasmon damping effects.

In this letter, we perform density-functional-theory molecular-dynamic (DFT-MD) simulations of the dynamic electrical conductivity of isochorically heated aluminum. The simulations include electron-electron interactions by the commonly used exchange-correlation (XC) functional of Perdew, Burke, and Enzerhof (PBE) [47] and the recently developed XC functional of Heyd, Scuseria, and Enzerhof (HSE) [48]. The resulting conductivity of both functionals show significant discrepancies. By comparing with new accurate angularly- and spectrally-resolved scattering measurements from LCLS, we found, for the first time, a very good agreement between the complete X-ray Thomson scattering spectrum including

This material is based upon work supported by the U.S. Department of Energy, Office of Science, under Contract No. DE-AC02-76SF00515.

all contributions that validate our full scale simulations with HSE. Moreover, our experimental data and simulations allow the experimental observation and theoretical interpretation of nonlinearly damped plasmons where the plasmon width is smaller than predicted by the RPA indicating non-Drude conductivities [49]. Previous investigations have studied non-Drude behavior due to localization of bound atomic states in expanding low-density plasmas [28, 50]. In contrast at solid density, WDM conditions we find that the conductivity is affected by excitations in the conduction band. This leads to a Cooper minimum [51] and non-linear plasmon damping that we observe via high-precision x-ray Thomson scattering.

The dynamic electrical conductivity $\sigma(\omega)$ and the DSF $S_{\mathrm{ee}}(k,\omega)$ are calculated from the ion number density and the single electron wave-functions [28, 33, 36, 52]. Both quantities are derived from DFT-MD, implemented within the Vienna Ab initio Simulation Package (VASP) [53–55] which is well-suited for the study of WDM. Here, the forces between the particles are calculated according to the Hellmann-Feynman theorem in each time step from the DFT calculations of the electronic structure by solving the Kohn-Sham equations. A projector augmented-wave potential [56] is applied, which considers the two inner K-shell electrons of the aluminum atom as frozen in the core, whereas the eleven L- and M-shell electrons are treated within the DFT framework. This potential allows excitations of M- and L-shell electrons. For the plane wave expansion of the Kohn-Sham wave functions we found convergence at a cutoff energy of 500 eV. For the exchange interactions and correlations, we use the approximation of PBE [47] and HSE [48]. The latter replaces one quarter of the short range PBE exchange with screened non-local Fock exchange [38]. The ionic subsystem is propagated via a classical MD algorithm. All MD simulations use 64 ions and are realized for at least 10000 time steps of 2 fs duration after equilibration. The particle temperature is controlled with a Nosé thermostat [57].

Figure 1 shows the dynamic electrical conductivity derived from the DFT-MD simulations and the corresponding Drude fit at a temperature of $T_i = T_e = 0.3$ eV and density of $\rho = 2.7$ g/cm^3. The calculations use the Kubo-Greenwood formula [60, 61] that applies electronic interband transitions from DFT [52] evaluated at the Baldereschi mean-value point [62]. The convergence of our simulations regarding the k-points is tested by using a $4 \times 4 \times 4$ Monkhorst-Pack grid. The conductivity represents an average over 20 independent ionic configurations obtained by MD simulations. For the Drude fits, we use $\mathrm{Re}\,\sigma(\Delta E) = \mathrm{Re}\left[\varepsilon_0 \omega_{\mathrm{pl,e}}^2 / \left(\nu - i\Delta E/\hbar\right)^2\right]$, with the plasma frequency $\omega_{\mathrm{pl,e}}$ and the static relaxation frequency ν [30]. For energy transfers $\Delta E < 21$ eV $= \Delta E_{\mathrm{excit}}$, the conductivity is fit well by this approximation. However, for energy transfers above $\Delta E_{\mathrm{excit}}$,

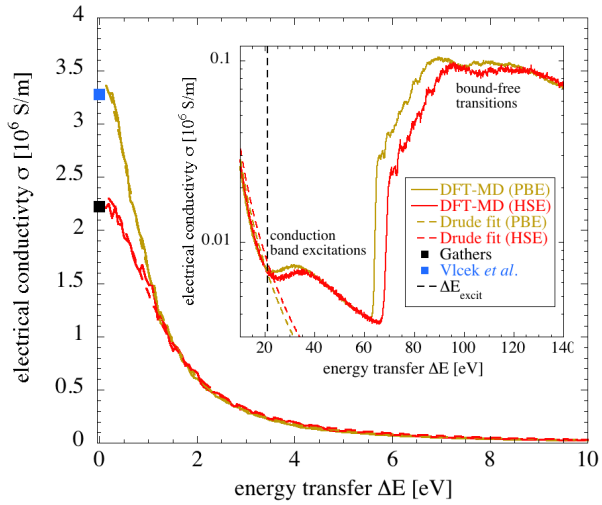

FIG. 1. Dynamic electrical conductivity in aluminum calculated from DFT-MD simulations at a temperature of $T_e = T_i = 0.3$ eV. The calculated conductivity is strongly dependent on the XC functional. dc conductivities of comparable previous simulations [58] (blue square) agrees with our PBE DFT simulations (gold line). In contrast, direct measurements [59] (black square) can only be described by our HSE DFT conductivities (red line). The non-Drude-like behavior, apparent in the inset, is caused by electronic excitations, which become significant for energy transfers $\Delta E > 21$ eV $= \Delta E_{\mathrm{excit}}$ as indicated (broken line), cf. Drude fit to the simulations (red and gold broken lines). The Drude and non-Drude behavior are well-separated by the Cooper minimum [51].

electronic transitions within the conduction band result in a non-Drude-like behavior [49], cf. inset of Fig. 1. For higher energy transfers $\Delta E > 60$ eV, bound-to-free electron transitions occur. For the conditions considered here, the dc conductivity $\sigma_{\mathrm{dc}} = \sigma(\Delta E \to 0)$ is strongly dependent on the XC functional used. Our conductivities calculated from DFT by using the PBE functional are in agreement with previous simulations [58]. However, directly measured dc conductivities ($\sigma_{\mathrm{dc}}^{\mathrm{exp}} = 2.22 \times 10^6$ S/m) [59] can only be reproduced from our simulations by using the HSE functional ($\sigma_{\mathrm{dc}}^{\mathrm{HSE}} = 2.23 \times 10^6$ S/m), that was not achieved previously by DFT-MD simulations [28, 63]. The differences in the conductivity values can be understood by differences in the electronic density of states (DOS) and resulting dissipative effects.

Figure 2 shows the DOS $D(E)$ and the Fermi electron-state occupation $f(E)$. Contrary to the PBE functional, the DOS in the conduction band calculated with the HSE functional is reduced at the Fermi edge and shifted to smaller energies defining reduced kinetic electron energies and dc conductivities. In the inset of Figure 2, the DOS, calculated with the HSE functional, shows L-shell electrons in the s-orbital (p-orbital) that are downshifted by a total energy of $\Delta E_{\mathrm{so}} = 6.01$ eV ($\Delta E_{\mathrm{po}} = 4.15$ eV) when compared to the PBE results. Consequently, the

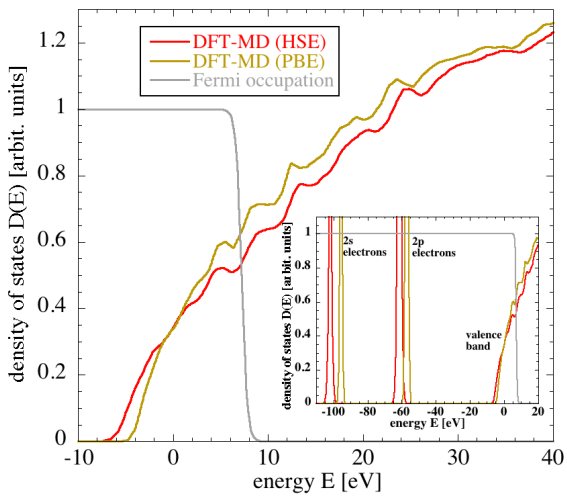

FIG. 2. DOS and Fermi occupation numbers in aluminum at a temperature of $T_i = T_e = 0.3$ eV. The DFT-MD simulations use PBE and HSE functionals. The inset shows the conduction band and the location of the L-shell electrons.

HSE calculations predict larger ionization energies consistent with Ref. [64]. This ionization energy discrepancy explains the energy-shift between the HSE and PBE calculated bound-free excitations observed in Fig. 1 at an energy of 68.9 eV (64.65 eV) in case of HSE (PBE). Previous bound-free excitation measurements on cold aluminum found energies of 72.7 eV [49].

An important prediction of the non-Drude behavior seen in the DFT-MD simulations are strong effects on the damping of plasmons with energies in the range of $\Delta E = 20$ eV $\approx \Delta E_{\text{excit}}$. Previous studies [22, 43, 65] calculated the plasmon damping via the Mermin approximation together with static local field corrections [66, 67] (MA) applying collision frequencies based on perturbative approximations [39, 44, 68]. Especially in strongly correlated systems, this analysis cannot provide satisfactory agreement with the detailed shape of the experimental scattering data [22].

Here, we apply our *ab initio* simulations in order to calculate the corresponding x-ray scattering spectra via the DSF that reflects the entire electronic structure and is usually described by the Chihara formula [39, 69–71]. The elastic scattering contribution arises from weakly and tightly bound electrons and is expressed in $|N(k)|^2 S_{\text{ii}}(k)$; it is sensitive to the ionic structure factor $S_{\text{ii}}(k)$ and the total electronic form factor $N(k)$. The total form factor can be derived from our DFT-MD simulated ion number density and single-electron wavefunctions [33]. The autocorrelation function of the ion number density provides the ionic structure factor [36]. Inelastic scattering on free and bound electrons causes electronic state transitions, that are included in our simulated dynamic electrical conductivity $\sigma(\omega)$. Applying the

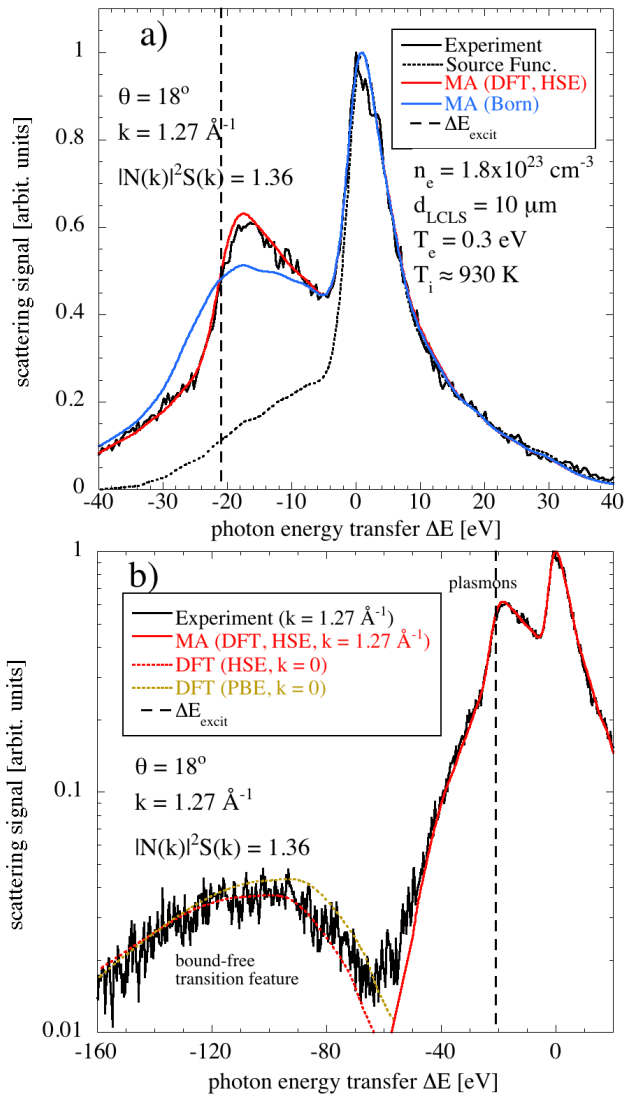

FIG. 3. Measured and calculated scattering spectra of aluminum illustrating a) the influence of the DFT-MD simulations and b) the dependence on the functional used within the DFT. The inelastic scattering is calculated from a perturbative approximation MA (Born) and our DFT-MD simulations using HSE and PBE functionals. The elastic scattering is calculated from our PBE DFT-MD simulations [33, 36]. The calculations are convoluted with the source function.

Kramers-Kronig relation, it is transformed into a complex dielectric function $\varepsilon^{\text{DFT}}(\omega, k = 0)$ [30] that defines the DSF via the fluctuation-dissipation theorem [39, 45]. In order to provide also the DSF for finite wavenumbers k, we apply the Mermin dielectric function ε^{M} [72, 73], valid for non-equilibrium systems [27], by using the complex relaxation frequency $\nu^{\text{DFT}}(\omega)$. The latter is calculated from our DFT-MD simulations by solving the equation $\varepsilon^{\text{M}}(\omega, k \to 0; \nu^{\text{DFT}}(\omega)) = \varepsilon^{\text{DFT}}(\omega, k \to 0; \nu^{\text{DFT}}(\omega))$ numerically [22].

Figure 3 shows the measured and calculated scatter-

ing spectra for a wavenumber of $k = 1.27$ Å^{-1}. Each measured spectrum is an average of 2000 shots. The spectra show an elastic scattering peak at the incident photon energy of $E = 7.98$ keV ($\Delta E = 0$), a pronounced plasmon resonance, downshifted by an energy transfer of $15-20$ eV, and a bound-free transition feature located at $\Delta E < -60$ eV. The plasmon scattering calculations use the MA applying relaxation frequencies from the Born approximation [22, 44] and our DFT-MD simulations. The bound-free transitions are derived directly from our DFT-MD simulated electrical conductivities at $k = 0$, see Fig. 1. The elastic scattering, plasmon and bound-free transition intensity are calculated without the use of any adjustments.

The ion temperature, $T_i = 930$ K, is inferred from the ion to plasmon feature intensity and is found to agree with all data at different wavenumbers. In addition, for these simulations we use electron temperatures, $T_e = 0.3$ eV, consistent with previous studies for similar conditions [22]. Here, the effect of non-equilibrium, $T_e \neq T_i$, is smaller than that due to the choice of the XC functional.

Considering the spectra calculated with DFT-MD relaxation frequencies in Fig. 3 a), we observe an agreement with the experimental data that is not achieved by the Born approximation [22]. Although the measured plasmon peak position agrees with results applying the Born approximation, the measured width is overestimated by these calculations. In contrast, our DFT-MD simulations show excellent agreement with both the measured scattering signal in the plasmon peak position and the width.

Moreover, in Fig. 3 b), our HSE DFT-MD results achieve a good agreement with the measured bound-free transition shape and plasmon to bound-free transition intensity ratio. In comparison, the PBE DFT-MD simulations show poor agreement with the data. This XC functional dependence is caused by the DOS, cf. Fig. 2, since the bound-free transition feature represents a weighted map of the DOS.

Figure 4 shows the measured and calculated plasmon width. Both the RPA that only includes Landau damping as dissipative effect as well as the MA, considering additional binary collisions in Born approximation, overestimates the plasmon width strongly. In contrast, the MA including dissipative processes in the full many-body description of DFT-MD agrees with the data for all wavenumbers (red curve). We conclude that the experimentally observed plasmon damping is reduced in comparison to the RPA due to additional conduction band excitations that become significant for energy transfers above $\Delta E_{\text{excit}} = 21$ eV (broken line in Figs. 1, 3). Note, that Landau damping (RPA) is still present but is modified by frequency-dependent damping through electron excitations. The inset shows the plasmon peak position (dispersion) as a function of the wavenumber k. The plasmon dispersion relation of the spectra applying relaxation frequencies in Born approximation and from DFT-MD simulations with HSE functionals agrees with the data best. The RPA (Landau damping) overestimates the dispersion for higher wavenumbers [65].

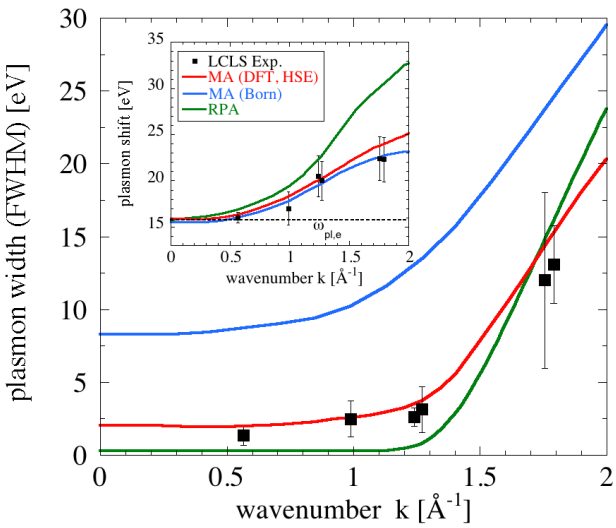

FIG. 4. Measured (black squares) and calculated plasmon width and peak position (inset) as a function of the wavenumber k for a temperature of 0.3 eV and LCLS focal spot sizes of 10 μm. The RPA (green line) neglects collisions but includes Landau damping. The MA considers collisions by using relaxation frequencies from the Born approximation (blue line) and from DFT-MD simulations with the HSE functional (red line).

In conclusion, we have calculated the electrical conductivity of warm dense aluminum at densities of $\rho = 2.7$ g/cm^3 from DFT-MD simulations using PBE and HSE XC functionals. The conductivities reveal non-Drude-like behavior induced by electron excitations in the conduction band. The conductivities yield the x-ray scattering spectra that compare well with measured data. The plasmon damping derived from our DFT-MD simulations is smaller compared to the widely used RPA. This deviation has to be studied in future work in the context of non-linear Landau damping. On the other hand, the RPA and the MA using Born collision frequencies calculate larger plasmon width due to an inaccurate description of dissipative processes in strongly coupled plasmas. This deficit shows that a full many-body description as provided by DFT is needed to reproduce highly accurate experimental measurements to understand optical properties in WDM.

We thank K. Burke, M. French, V. Recoules, H. Reinholz, and G. Röpke for helpful discussions. The experiments were performed at the MEC instrument of LCLS, supported by the DOE Office of Science, Fusion Energy Science under Contract No. SF00515. The work was supported by the DOE Office of Science, Fusion Energy Science under FWP 100182 and the DFG within the

SFB 652. The work was further supported by a Laboratory Directed Research and Development grant, the Alexander von Humboldt Foundation, and the Volkswagen Foundation.

[1] D. Kremp, M. Schlanges, and W.-D. Kraeft, Quantum Statistics of Nonideal Plasmas (Springer Verlag, Berlin, 2005).
[2] S. Ichimaru, Statistical Plasma Physics Vol. II: Condensed Plasmas (Addison-Wesley Publishing Co., Reading, 1994).
[3] C. Villani, Phys. Plasmas **21**, 030901 (2014).
[4] J. H. Malmberg and C. B. Wharton, Phys. Rev. Lett. **13**, 184 (1964).
[5] C. Mouhot and C. Villani, J. Math. Phys. **51**, 015204 (2010).
[6] R. L. Berger, S. Brunner, T. Chapman, L. Divol, C. H. Still, and E. J. Valeo, Phys. Plasmas **20**, 032107 (2013).
[7] R. Redmer, T. R. Mattsson, N. Nettelmann, and M. French, Icarus **211**, 798 (2011).
[8] T. R. Mattsson and M. P. Desjarlais, Phys. Rev. Lett. **97**, 017801 (2006).
[9] M. French, A. Becker, W. Lorenzen, N. Nettelmann, M. Bethkenhagen, J. Wicht, and R. Redmer, Astrophys. J. Suppl. Ser. **202**, 11 (2012).
[10] P. Olson, Science **342**, 431 (2013).
[11] J. D. Lindl, P. Amendt, R. L. Berger, S. G. Glendinning, S. H. Glenzer, S. W. Haan, R. L. Kauffman, O. L. Landen, and L. J. Suter, Phys. Plasmas **11**, 339 (2004).
[12] P. Davis, T. Döppner, J. R. Rygg, C. Fortmann, L. Divol, A. Pak, L. B. Fletcher, A. Becker, B. Holst, P. Sperling, R. Redmer, M. P. Desjarlais, P. Celliers, G. W. Collins, O. L. Landen, R. W. Falcone, and S. H. Glenzer, Nat. Comm. **7**, 11189 (2016).
[13] B. Hammel, S. Haan, D. Clark, M. Edwards, S. Langer, M. Marinak, M. Patel, J. Salmonson, and H. Scott, High Energy Dens. Phys. **6**, 171 (2010).
[14] A. W. DeSilva and H.-J. Kunze, Phys. Rev. E **49**, 4448 (1994).
[15] A. Ng, P. Celliers, A. Forsman, R. M. More, Y. T. Lee, F. Perrot, M. W. C. Dharma-wardana, and G. A. Rinker, Phys. Rev. Lett. **72**, 3351 (1994).
[16] A. N. Mostovych and Y. Chan, Phys. Rev. Lett. **79**, 5094 (1997).
[17] A. W. DeSilva and J. D. Katsouros, Phys. Rev. E **57**, 5945 (1998).
[18] I. Krisch and H.-J. Kunze, Phys. Rev. E **58**, 6557 (1998).
[19] J. F. Benage, W. R. Shanahan, and M. S. Murillo, Phys. Rev. Lett. **83**, 2953 (1999).
[20] V. N. Korobenko, A. D. Rakhel, A. I. Savvatimski, and V. E. Fortov, Phys. Rev. B **71**, 014208 (2005).
[21] K. Y. Kim, B. Yellampalle, J. H. Glownia, A. J. Taylor, and G. Rodriguez, Phys. Rev. Lett. **100**, 135002 (2008).
[22] P. Sperling, E. J. Gamboa, H. K. Chung, E. Galtier, H. J. Lee, Y. Omarbakiyeva, H. Reinholz, G. Röpke, U. Zastrau, J. Hastings, L. B. Fletcher, and S. H. Glenzer, Phys. Rev. Lett. **115**, 115001 (2015).
[23] J. Clerouin, C. E. Starrett, G. Faussurier, C. Blancard, P. Noiret, and P. Renaudin, Phys. Rev. E **82**, 046402 (2010).
[24] Z. Konôpková, R. S. McWilliams, N. Gómez-Pérez, and A. F. Goncharov, Nature **534**, 99 (2016).
[25] T. Sjostrom and J. Daligault, Phys. Rev. E **92**, 063304 (2015).
[26] L. B. Fletcher, H. J. Lee, T. Döppner, E. Galtier, B. Nagler, P. Heimann, C. Fortmann, S. LePape, T. Ma, M. Millot, A. Pak, D. Turnbull, D. A. Chapmann, D. O. Gericke, J. Vorberger, T. White, G. Gregori, M. Wei, B. Barbrel, R. W. Falcone, C.-C. Kao, H. Nuhn, J. Welch, U. Zastrau, P. Neumayer, J. B. Hastings, and S. H. Glenzer, Nat. Photonics **9**, 274 (2015).
[27] P. Sperling, S. Rosmej, R. Bredow, L. B. Fletcher, E. Galtier, E. J. Gamboa, H.-J. Lee, H. Reinholz, G. Röpke, U. Zastrau, and S. H. Glenzer, submitted to J. Phys. B (2016).
[28] M. P. Desjarlais, J. D. Kress, and L. A. Collins, Phys. Rev. E **66**, 025401 (2002).
[29] C. E. Starrett, J. Clerouin, V. Recoules, J. D. Kress, L. A. Collins, and D. E. Hanson, Phys. Plasmas **19**, 102709 (2012).
[30] K.-U. Plagemann, P. Sperling, R. Thiele, M. P. Desjarlais, C. Fortmann, T. Döppner, H. J. Lee, S. H. Glenzer, and R. Redmer, New J. Phys. **14**, 055020 (2012).
[31] M. D. Knudson, M. P. Desjarlais, A. Becker, R. W. Lemke, K. R. Cochrane, M. E. Savage, D. E. Bliss, T. R. Mattsson, and R. Redmer, Science **348**, 1455 (2015).
[32] C. E. Starrett, J. Daligault, and D. Saumon, Phys. Rev. E **91**, 013104 (2015).
[33] K.-U. Plagemann, H. R. Rüter, T. Bornath, M. Shihab, M. P. Desjarlais, C. Fortmann, S. H. Glenzer, and R. Redmer, Phys. Rev. E **92**, 013103 (2015).
[34] T. Schoof, S. Groth, J. Vorberger, and M. Bonitz, Phys. Rev. Lett. **115**, 130402 (2015).
[35] J. Daligault, S. D. Baalrud, C. E. Starrett, D. Saumon, and T. Sjostrom, Phys. Rev. Lett. **116**, 075002 (2016).
[36] H. R. Rüter and R. Redmer, Phys. Rev. Lett. **112**, 145007 (2014).
[37] A. Benuzzi-Mounaix, F. Dorchies, V. Recoules, F. Festa, O. Peyrusse, A. Levy, A. Ravasio, T. Hall, M. Koenig, N. Amadou, E. Brambrink, and S. Mazevet, Phys. Rev. Lett. **107**, 165006 (2011).
[38] A. D. Baczewski, L. Shulenburger, M. P. Desjarlais, S. B. Hansen, and R. J. Magyar, Phys. Rev. Lett. **116**, 115004 (2016).
[39] S. H. Glenzer and R. Redmer, Rev. Mod. Phys. **81**, 1625 (2009).
[40] Y. Ding, A. Brachmann, F.-J. Decker, D. Dowell, P. Emma, J. Frisch, S. Gilevich, G. Hays, P. Hering, Z. Huang, R. Iverson, H. Loos, A. Miahnahri, H.-D. Nuhn, D. Ratner, J. Turner, J. Welch, W. White, and J. Wu, Phys. Rev. Lett. **102**, 254801 (2009).
[41] P. Emma, R. Akre, J. Arthur, R. Bionta, C. Bostedt, J. Bozek, A. Brachmann, P. Bucksbaum, R. Coffee, F. J. Decker, Y. Ding, D. Dowell, S. Edstrom, A. Fisher, J. Frisch, S. Gilevich, J. Hastings, G. Hays, Z. Hering, P. Huang, R. Iverson, H. Loos, M. Messerschmidt, A. Miahnahri, S. Moeller, H.-D. Nuhn, G. Pile, D. Ratner, J. Rzepiela, D. Schultz, T. Smith, P. Stefan, H. Tompkins, J. Turner, J. Welch, W. White, G. Yocky, and J. Galayda, Nat. photonics **4**, 641 (2010).
[42] S. H. Glenzer, L. B. Fletcher, E. Galtier, B. Nagler, R. Alonso-Mori, B. Barbrel, S. B. Brown, D. A. Chapman, Z. Chen, C. B. Curry, F. Fiuza, E. J. Gamboa, M. Gauthier, D. O. Gericke, A. Gleason, S. Göde, E. Granados, P. Heimann, J. Kim, D. Kraus, M. J.

MacDonald, A. J. Mackinnon, R. Mishra, A. Ravasio, C. Rödel, P. Sperling, W. Schumaker, Y. Y. Tsui, J. Vorberger, U. Zastrau, A. Fry, W. E. White, J. B. Hasting, and H. J. Lee, J. Phys. B **49**, 092001 (2016).

[43] S. H. Glenzer, O. L. Landen, P. Neumayer, R. W. Lee, K. Widmann, S. W. Pollaine, R. J. Wallace, G. Gregori, A. Höll, T. Bornath, R. Thiele, V. Schwarz, W.-D. Kraeft, and R. Redmer, Phys. Rev. Lett. **98**, 065002 (2007).

[44] H. Reinholz, R. Redmer, G. Röpke, and A. Wierling, Phys. Rev. E **62**, 5648 (2000).

[45] A. Höll, T. Bornath, L. Cao, T. Döppner, S. Düsterer, E. Förster, C. Fortmann, S. H. Glenzer, G. Gregori, T. Laarmann, K.-H. Meiwes-Broer, A. Przystawik, P. Radcliffe, R. Redmer, H. Reinholz, G. Röpke, R. Thiele, J. Tiggesbäumker, J. Toleikis, N. X. Truong, T. Tschentscher, I. Uschmann, and U. Zastrau, High Energy Dens. Phys. **3**, 120 (2007).

[46] R. Fäustlin, T. Bornath, T. Döppner, S. Düsterer, E. Förster, C. Fortmann, S. H. Glenzer, S. Göde, G. Gregori, R. Irsig, T. Laarmann, H. Lee, B. Li, K.-H. Meiwes-Broer, J. Mithen, B. Nagler, A. Przystawik, H. Redlin, R. Redmer, H. Reinholz, G. Röpke, F. Tavella, R. Thiele, J. Tiggesbäumker, S. Toleikis, I. Uschmann, S. Vinko, T. Whitcher, U. Zastrau, B. Ziaja, and T. Tschentscher, Phys. Rev. Lett. **104**, 125002 (2010).

[47] J. P. Perdew, K. Burke, and M. Ernzerhof, Phys. Rev. Lett. **77**, 3865 (1996).

[48] J. Heyd, G. E. Scuseria, and M. Enzerhof, J. Chem. Phys. **118**, 219906 (2003).

[49] E. M. Gullikson, P. Denham, S. Mrowka, and J. H. Underwood, Phys. Rev. B **49**, 16283 (1994).

[50] A. Lévy, F. Dorchies, A. Benuzzi-Mounaix, A. Ravasio, F. Festa, V. Recoules, O. Peyrusse, N. Amadou, E. Brambrink, T. Hall, M. Koenig, and S. Mazevet, Phys. Rev. Lett. **108**, 055002 (2012).

[51] S. T. Manson, Phys. Rev. A **31**, 3698 (1985).

[52] B. Holst, M. French, and R. Redmer, Phys. Rev. B **83**, 235120 (2011).

[53] G. Kresse and J. Hafner, Phys. Rev. B **47**, 558 (1993).

[54] G. Kresse and J. Hafner, Phys. Rev. B **49**, 14251 (1994).

[55] G. Kresse and J. Furthmüller, Phys. Rev. B **54**, 11169 (1996).

[56] P. E. Blöchl, Phys. Rev. B **50**, 17953 (1994).

[57] S. Nosé, J. Chem. Phys. **81**, 511 (1984).

[58] V. Vlček, N. de Koker, and G. Steinle-Neumann, Phys. Rev. B **85**, 184201 (2012).

[59] G. R. Gathers, Int. J. Thermophys. **4**, 209 (1983).

[60] R. Kubo, J. Phys. Soc. Jpn. **12**, 570 (1957).

[61] D. A. Greenwood, Proc. Phys. Soc. **71**, 585 (1958).

[62] A. Baldereschi, Phys. Rev. B **7**, 5212 (1973).

[63] V. Recoules and J. P. Crocombette, Phys. Rev. B **72**, 104202 (2005).

[64] M. French, T. R. Mattsson, and R. Redmer, Phys. Rev. B **82**, 174108 (2010).

[65] P. Neumayer, C. Fortmann, T. Döppner, P. Davis, R. W. Falcone, A. L. Kritcher, O. L. Landen, H. J. Lee, R. W. Lee, C. Niemann, S. Le Pape, and S. H. Glenzer, Phys. Rev. Lett. **105**, 075003 (2010).

[66] B. Farid, V. Heine, G. E. Engel, and I. J. Robertson, Phys. Rev. B **48**, 11602 (1993).

[67] C. Fortmann, A. Wierling, and G. Röpke, Phys. Rev. E **81**, 026405 (2010).

[68] H. Reinholz, G. Röpke, S. Rosmej, and R. Redmer, Phys. Rev. E **91**, 043105 (2015).

[69] J. Chihara, J. Phys. F **17**, 295 (1987).

[70] J. Chihara, J. Phys. Cond. Matter **12**, 231 (2000).

[71] G. Gregori, S. H. Glenzer, and O. L. Landen, J. Phys. A **36**, 597 (2003).

[72] N. D. Mermin, Phys. Rev. B **1**, 2362 (1970).

[73] G. Röpke, A. Selchow, A. Wierling, and H. Reinholz, Phys. Lett. A **260**, 365 (1999).